Wave functions in the critical phase: A planar Sierpiński fractal lattice

Qi Yao [1,2,*] Xiaotian Yang [3,*] Askar A. Iliasov [4] Mikhail I. Katsnelson [5] and Shengjun Yuan [3,6,†]

[1] *Quantum Science Center of Guangdong-Hong Kong-Macao Greater Bay Area (Guangdong), Shenzhen 518045, China*

[2] *Institute of Quantum Precision Measurement, State Key Laboratory of Radio Frequency Heterogeneous Integration, College of Physics and Optoelectronic Engineering, Shenzhen University, Shenzhen 518060, China*

[3] *Key Laboratory of Artificial Micro- and Nano-structures of Ministry of Education and School of Physics and Technology, Wuhan University, Wuhan, Hubei 430072, China*

[4] *Department of Physics, University of Zurich, Winterthurerstrasse 190, 8057 Zurich, Switzerland*

[5] *Institute for Molecules and Materials, Radboud University, Heijendaalseweg 135, 6525 AJ Nijmegen, The Netherlands*

[6] *Wuhan Institute of Quantum Technology, Wuhan 430206, China*

(Received 24 April 2024; accepted 18 June 2024; published 1 July 2024)

Electronic states play a crucial role in many quantum systems of moiré superlattices, quasicrystals, and fractals. As recently reported for Sierpiński lattices [Yao *et al.*, Phys. Rev. B **107**, 115424 (2023)], the critical states are revealed by the energy-level-correlation spectra, which are caused by the interplay between aperiodicity and determined self-similarity characters. In the case of the Sierpiński carpet, our results further demonstrate that there is some degree of spatial overlap between these electronic states. These states could be strongly affected by the "seed lattice" of the generator and slightly modulated by the dilation pattern and the geometrical self-similarity level. These electronic states are made multifractal by scaling the qth-order inverse participation ratio or fractal dimension, which correlates with the subdiffusion behavior. In the gene pattern, an average state-based multifractal dimension of second order would increase as its Hausdorff dimension increases. Our findings could potentially contribute to understanding quantum transports and single-particle quantum dynamics in fractals.

DOI: 10.1103/PhysRevB.110.035403

I. INTRODUCTION

Translational invariance of atomic arrangement in crystals leads to the band theory based on the Bloch theorem; the Bloch character of electronic wave functions describes an enormous number of properties of crystalline solids [1–5]. This symmetry is absent in randomly disordered systems [6–8] as well as in incommensurate (quasiperiodic) systems such as the one-dimensional (1D) Fibonacci chain [9], two-dimensional Penrose tiling [10,11], Ammann-Beenker lattice [12,13]), and hierarchical tiling of Sierpiński lattices [14–16] and Koch fractals [17]. In all these cases tools dramatically different from the band theory are required. In particular, the concept of Anderson localization [18] is necessary to understand the properties of disordered systems [6–8]. After many years of efforts, we have well-developed mathematical tools to describe this and related phenomena [19], and some of these tools will be named below. The cases of regular but not translationally invariant systems such as quasicrystals and fractals are much less studied, and we are still far from complete understanding of their electron properties.

To better study these aperiodic structures, many researchers have developed various alternative theoretical methods, including the renormalization group technique [20–28], transfer matrices [29–32], level-spectrum statistics [33] from random matrices theory [34,35], one-parameter scaling based on studies of correlated length for coherent structures of different sizes [36,37] or localized length [38] in the Anderson model [18,39], the state-based multifractality scaling [32], studying transport properties [40–42], etc.

Following the above timeline, two key objects, namely, energy spectra [33–35] and wave functions in real space [36,37], come into view that can be exploited to analyze electronic [43–45] and phonon [46] systems. For instance, the wave functions belong to one of three types: the characteristically (Bloch) extended state [4] in periodicity-translation crystals; the typically localized state [18] in systems with disorder induced by impurities, defects, etc.; and a state behaving in between that remains critical in several quasicrystals like the Fibonacci chain [47], Thue-Morse lattice [48], and some Penrose tilings [49]. In general, these can be distinguished as follows: whereas the localized wave functions have an exponentially localized envelope with $|\psi(r)| \sim \exp(-\alpha r^{\beta})$, where α and β are the spatial parameters, the decay of the critical states follows a power-law form with $|\psi(r)| \sim |r|^{-\alpha}$ (or a more complicated envelope, e.g., localized edge states in a ring shape [43] and critical states with the SKK form in Penrose lattices [44]). Note that *in the absence of disorder*, lattice frustration possibly induces the fragmented states (i.e., critical states) in quasicrystals and fractals; these states also become more complex with various long-range orders.

Sierpiński carpets SC(n, m, g^*) as a class of fractals [14,50–53], where (n, m) are the parameters of the generator(n, m) and g^* is the geometrical hierarchy level,

*These authors contributed equally to this work.
†Contact author: s.yuan@whu.edu.cn

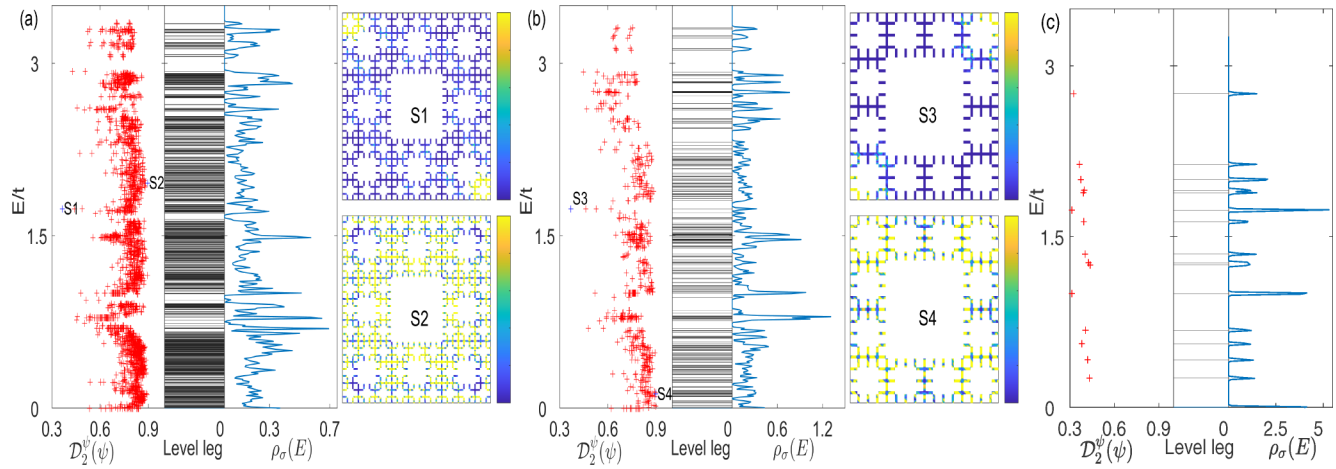

FIG. 1. Schematic illustration of the SC(n, m, g^*) fractal lattices by a paradigmatic generator$(4, 2)$ under the (a) self, (b) gene, and (c) auxiliary vari patterns. Geometrical hierarchy level $g^* = 3$. Energy spectra are symmetric about $E = 0$; hence, the upper half panel of the energy spectra is considered, i.e., $0 \leqslant E \leqslant 4t$. In the main panel in (a), (b), and (c), the fractal dimension $\mathcal{D}_2^{\psi}(\psi)$ (red crosses, shown on the left) of the wave function measures its degree of spatial extension in the whole lattice; the level leg E (black line in the middle) and density of states $\rho_\sigma(E)$ (blue curve on the right) with a blurred energy width $\sigma = 0.0056t$ [74] are also shown. Two extreme (minimum and maximum) cases of $\mathcal{D}_2^{\psi}(\psi)$ give four states, which are marked in blue with S1 and S3 (S2 and S4) in the top (bottom) right panels. The scaled probability density $Ar|\psi_{E_n}(i)|^2$ maps into a color bar region from 0 to Ar.

resemble a periodic square lattice in two dimensions, whose order of ramification is infinite. Experimentally, these fractal objects can be accessed by arranging a waveguide tube [54] and electric circuit [55] or printing acoustic lattices [56] in desired fractal shapes [14,57]. In Ref. [58], we found that when a single electron roams upon the SC(n, m, g^*) lattices, all electronic states reside in the critical phase, which isolates that near the mobility edge where Anderson transition occurs [39]. This trait affects the observable properties of quantum conductance (QC) [59] and QC-based box-counting dimensions, plasmas [60], and Hall conductance [61], among others.

To obtain more insight into fractal lattices, we focus on probing the spatial envelope of electronic states, rather than the nearest energy-correlation spectra. Two aspects are studied: (1) the state envelope in these SC(n, m, g^*) lattices at various energy bands and (2) how other factors, such as the generator(n, m), dilation pattern, fractal dimension $\mathcal{D}_H$, and geometrical hierarchy level g^*, affect the critical states (CSs). Critical states are potentially crucial for further investigating the disorder-induced localization [62] and many-body correlation effect [63] in Sierpiński fractal lattices.

The rest of this paper is organized as follows. In Sec. II, we introduce the single-electron gas model on the SC(n, m, g^*) lattices and the state-based multifractality analysis. Our results are presented in Sec. III. For three lattice-dilation patterns with SC$(n, m, 3)$ lattices, the electronic states are sketched by their density profile in Sec. III A, and their multifractal properties are shown in Sec. III B. A conclusion is reached in Sec. IV.

II. LATTICE, MODEL, AND METHOD

Fractal lattices and model. First, we review the fractal SC(n, m, g^*) lattices that we discussed previously (see Fig. 1 in Ref. [58]). Using the generator(n, m) and two illustrations of the self and gene patterns ($M_{\rm se}$ and $M_{\rm ge}$), various SC(n, m, g^*) lattices are dilated. Here, these two patterns are our main interest, with the addition of the vari pattern, which is a variation of the self pattern, for comparison. Second, a noninteracting electron gas is confined in the SC(n, m, g^*) lattices, which is modeled by

$$H = -t \sum_{\langle i,j \rangle} (\mathbf{c}_i^\dagger \mathbf{c}_j + \mathbf{c}_j^\dagger \mathbf{c}_i) + V \sum_i f(i) \mathbf{c}_i^\dagger \mathbf{c}_i. \tag{1}$$

The first term describes a single electron hopping between the nearest-neighbor site pair $\langle i, j \rangle$. We set the strength t as the energy unit. The on-site potential with strength V included in the second term is tailored locally by the function $f(i)$ in the Anderson [18], Harper [64], Aubry or Aubry-André [65], and Aubry-André-Harper [65,66] models. Third, for consistency with Ref. [58], taking only the lattice topology effect into account, we set $V = 0$. The results of the level-spectrum statistics indicate that the electronic states might be intermediately critical (in other words, they always partially occupy the entire lattice, or the tail of the level-correlation spectra follows the power-law trait). We further use this tool to quantify these electronic states.

State-based multifractality analysis. For an arbitrary state ψ, measuring its spatial extension in a lattice as a convenient tactic can reveal some inherent traits, which are exploited in studying the localization problem with several concepts such as localization length [67,68], structural entropy [69,70], participation ratio [70], and multifractality [32]. We adopt the $2q$-norm multifractality [32] with the formula

$$\chi_q(\psi, \Omega) = \frac{\sum_{i \in \mathcal{R}} |\psi(i)|^{2q}}{\left(\sum_{i \in \mathcal{R}} |\psi(i)|^2\right)^q}, \tag{2}$$

with $\chi_q(\psi, \Omega)$ being the qth-order inverse participation ratio (IPR), where Ω is the number of sites counted in region $\mathcal{R}$.

To understand Eq. (2) well, we take three examples: (1) One of the wave functions is evenly extended in the spatial

lattice, i.e., $\psi(r) = \text{const}$; then we have $\chi_q(\psi, \Omega) = \Omega^{1-q}$, with Ω being the lattice size. (2) Assuming $\psi(r)$ have a power-law-decay envelope with an exponent α, instead,

$$\chi_q(\psi, \Omega) \simeq \begin{cases} \Omega^{-2(q-1)} & (0 \leqslant \alpha < 1/q), \\ \Omega^{-2q(1-\alpha)} & (1/q \leqslant \alpha < 1), \\ \Omega^0 & (1 \leqslant \alpha) \end{cases} \tag{3}$$

for $q > 1$. (3) The last example has an envelope of exponential decay and an oscillation tail, namely, the localized state. If the third state continues to degenerate highly and occupies only several sites, we refer to it as the confined state. One might imagine a state with a single occupied site, which would obviously have $\chi_q(\psi, \mathcal{R}) = 1$. Note that $\chi_q(\psi, \mathcal{R})$ clearly depends on the region $\Omega(\mathcal{R})$ one computes. Because different states are associated with lattices of various sizes, it becomes tricky to compare these electronic states directly.

However, using $\mathcal{D}_q^{\psi}(\psi)$ could avoid this issue. Since the quantity $\chi_q(\psi, \mathcal{R})$ scales exponentially as $\mathcal{R}^{-(q-1)\mathcal{D}_q^{\psi}(\psi)}$, which is linked the qth fractal dimension [71],

$$\mathcal{D}_q^{\psi}(\psi) = \lim_{\mathcal{R}\to\infty} \frac{-1}{q-1} \frac{\log \chi_q(\psi(i), \mathcal{R})}{\log \Omega(\mathcal{R})}. \tag{4}$$

In general, the second-order quantities of $q = 2$ demarcate the extended (localized) state with $\chi_2(\psi) = \Omega^{-1}$ and $\mathcal{D}_2^{\psi}(\psi) = 1$ [$\chi_2(\psi) \simeq 1$ and $\mathcal{D}_2^{\psi}(\psi) \simeq 0$]. There is a special situation where our observed values are in between, leading the system to a critical state. This can happen in two scenarios. One is near the mobility edge when Anderson transition occurs [72,73]. The other scenario is found in quasicrystals [32], where geometric frustration plays a role. In both cases, the electronic states are spatially fragmented differently.

Our work mainly explores the CSs within fractals. It is interesting to note that when two CSs are close in characteristics, we can spot the differences between them by measuring the IPR $\chi_q(\psi, \mathcal{R})$ and the state-based fractal dimension $\mathcal{D}_q^{\psi}(\psi)$, especially when using a higher value of q. This aspect becomes crucial when we observe the vast clustering of CSs in the spectra of $\mathcal{D}_q^{\psi}(\psi)$.

III. RESULTS AND DISCUSSION

In this section, we study the critical states from different perspectives. These include (1) examining their density profile, which helps us understand how the wave function occupies the entire fractal lattice, akin to analyzing the IPR, and (2) investigating the multifractality scaling (fractal dimension), which is related to the subdiffusion behaviors and can be observed by the dynamical evolutions in larger fractals.

A. The density profile on three SC(n, m, 3) lattices

To highlight how the CSs in fractal lattices are distinct from the other two types of states (extended and localized), we start by examining their spatial density profiles. We demonstrate this using three examples of SC$(4, 2, g^* = 3)$ lattices. These lattices are designed sequentially following specific patterns: the self pattern, with a matrix $M_{\text{se}} = [1\ 1\ 1; 1\ 0\ 1; 1\ 1\ 1]$; the gene pattern, with $M_{\text{ge}} = [1\ 1\ 1\ 1; 1\ 0\ 0\ 1; 1\ 0\ 0\ 1; 1\ 1\ 1\ 1]$; and the vari pattern, a variation of the self pattern, with $M_{\text{va}} = [1\ 0\ 0; 0\ 0\ 1; 1\ 1\ 0]$. Note that in the M_{ge} pattern, 1 means that the seed lattice of the generator(n, m) is filled; otherwise, it is not filled. The other two patterns are similar. The first two patterns (M_{se} and M_{ge}) are our primary focus, and the third one serves as a variant to emphasize the potential enhancement effect of local energy clusters (refer to Fig. S1 in our previous work [58]).

The level leg in Fig. 1 demonstrates that several critical states form a subband cluster, influenced by specific parameters such as the generator(n, m), the geometrical hierarchy level g^*, and the dilation patterns represented by matrices M_{se} and M_{ge}. This formation is discussed further in Ref. [58]. Moreover, the clustering degree of these levels is quantified using the density of states $\rho_\sigma(E)$ [74], where variations in the width and height of the peak indicate the presence of quasidegenerate and degenerate states, respectively. Notably, the self pattern exhibits a more pronounced level clustering.

Despite the energy level clustering, each subband possesses a detailed internal structure, which is particularly noticeable at specific in-band positions and can be described using multifractal energy spectra [32,75]. Instead of focusing solely on these spectra, our analysis utilizes q-weight scaling related to the wave function to examine the spatial differences between any two states. The spatial density of these CSs is illustrated using the scaled state density $Ar|\psi_{E_n}(i)|^2$, with the scaling factor Ar corresponding to the lattice size.

Moreover, it must be stressed that a small energy-resolved window δ (approximately $10^{-3}t$) is used to depict the states within specific energy clusters accurately. This approach averages all states within the energy range $E_n \pm \delta/2$, highlighting the (quasi)degenerate behavior in specific energy clusters. At the same time, it is used for subdiffusion behavior [76], such as benchmarking the autocorrelation function and mean-square displacement of the critical states in different lattices [77–80]. These tools, including the energy-correlation spectra [58], are equivalent in capturing the energy spectra or states in statistical views. Here, we analyze each state one by one.

The second-order fractal dimension $\mathcal{D}_2^{\psi}(\psi_E)$ for all states in two SC(4, 2, 3) lattices, associated with the self and gene patterns, typically ranges between 0.6 and 0.9. The proportion of states within this range is 0.974 and 0.937 for these two patterns, respectively. States outside this range are rare, indicating that the wave functions are predominantly critical. Figures 1(a) and 1(b) illustrate four eigenstates with extreme values of $\mathcal{D}_2^{\psi}(\psi_E)$, showcasing the characteristic of partial occupancy in fractals and the spatial overlap between these states.

The eigenstates labeled S1, S2, S3, and S4 exhibit a semblance of approximate symmetry, likely resulting from spontaneous symmetry breaking. This characteristic remains consistent across various CSs and in different SC(n, m, g^*) lattice configurations. However, these symmetrical traits in the spatial wave function are not universally applicable to most CSs, as evidenced by G4 in Fig. 3 below.

For the vari pattern, the fractal dimension $\mathcal{D}_2^{\psi}(\psi_E)$ is around 0.3, as shown in Fig. 1(c), which is notably low. This anomaly is primarily attributed to the substantial number of nonconnecting site subclusters scattered throughout the entire lattice, which are dilated according to the vari pattern. This

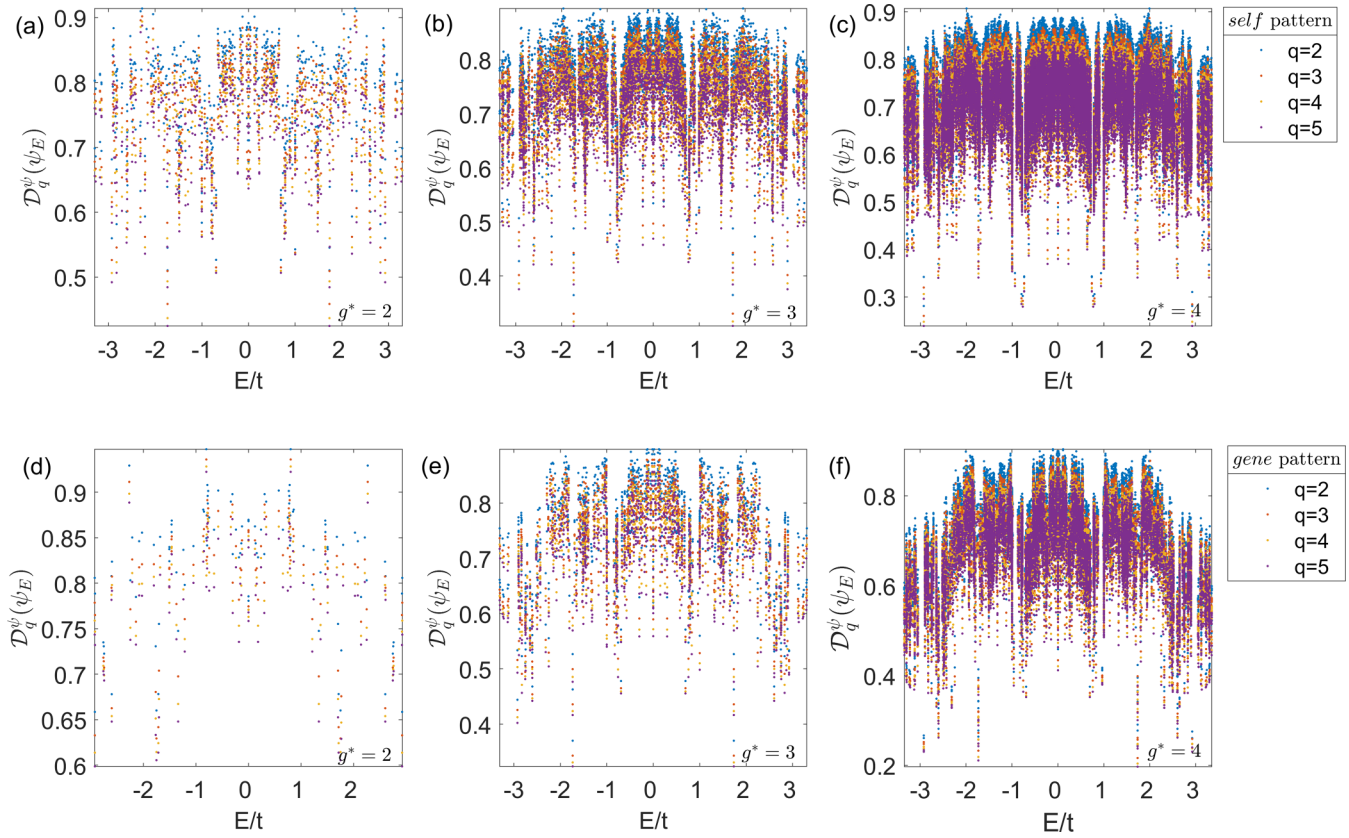

FIG. 2. The qth-order fractal dimension $\mathcal{D}_q^\psi(\psi_E)$ vs critical state $\psi_E(i)$ at allowed eigenenergy E. In order to capture the impact of the dilation pattern, we still use the generator(4, 2) as a case. Considering the geometrical hierarchy effect in Ref. [58], we modulate g^* from 2 to 4 for (a)–(c) the self pattern and (d)–(f) the gene pattern. Here, q goes from 2 to 5.

structural feature reduces the connectivity and interference across the lattice, resulting in the significantly lower fractal dimension observed.

To make an analogy, we recall some electrical states in quasicrystals [81]. First, taking the 1D Fibonacci chain [32] case, some electronic states at the band center are self-similar and critical, having $\psi_m \propto (1/N)^{\alpha_E}$ (where α_E is the exponent index [47,82]). Second, the situations become different in the Penrose lattice (space dimension $D = 2$); confined states [83,84] and self-similar states [83] exist in special tiling alignments. Third, in the Amman-Kramer lattice ($D = 3$), the electronic states are also critical and show power-law decay [85]. $\mathcal{D}_q^\psi(\psi_E)$ for electronic states in quasicrystals is less than $D/2$; the value of D depends on the space dimension where the quasicrystals are nested. $\mathcal{D}_q^\psi(\psi_E)$ is less than 1 in Sierpiński fractals, and it is closer to the fractal dimension $\mathcal{D}$. Additionally, the quasicrystals are lacuna-free; however, the fractals have lots of lacunae [86,87]. Hence, the typical power-law character of some critical states is almost absent in fractals.

B. The multifractality analysis in the SC(n, m, g^*) lattices

For multifractal critical states, we can utilize the state-based fractal dimension $\mathcal{D}_q^\psi(\psi_E)$ to characterize their distinctive features, notably how the value of $\mathcal{D}_q^\psi(\psi_E)$ varies with the scaling parameter q [32,88–92]. Unless otherwise specified in this paper, the entire fractal lattice (where Ar denotes the fractal lattice size) is always considered; hence, $\Omega = Ar$ is set. Generally, electronic states exhibit different behaviors when a single electron is situated at various energy levels, resulting in $\mathcal{D}_q^\psi(\psi_E)$ being dependent on the energy E, as depicted in Fig. 2. The hole-particle symmetry further makes $\mathcal{D}_q^\psi(\psi_E)$ symmetric around $E = 0$ across the entire spectrum of $\mathcal{D}_q^\psi(\psi_E)$. In the following, we study how these CSs change with the geometrical hierarchy level g^*, the two dilation types of the self and gene patterns, and the generator(n, m). First, we assess the influence of the geometric hierarchy level g^*, which is pivotal for self-similarity objects. In Figs. 2(a)–2(c), we select the generator(4, 2) as the case. In the self pattern, the q-weighted fractal dimension $\mathcal{D}_q^\psi(\psi)$ remains between 0.5 and 0.85 when $g^* = 2$ in Fig. 2(a); when g^* increases to 3, $\mathcal{D}_q^\psi(\psi)$ undergoes slight adjustments but generally stays within the same range, as shown in Fig. 2(b). Concurrently, many CSs cluster closely in the energy band and overlap within the spatial lattice, a phenomenon induced by the level attraction effect of g^*. As g^* increases to 4, the maximum value we can simulate, the profiles of $\mathcal{D}_q^\psi(\psi)$ in Fig. 2(c) resemble those at $g^* = 3$.

We turn to the gene pattern, for which g^* varies from 2 to 4, the entire span of $\mathcal{D}_q^\psi(\psi)$ narrows, and the distinct subclusters become apparent [refer to Figs. 2(d)–2(f)]. This effect is presumably due to the strong correlations between the CSs, whose energy levels are closely aligned, possibly leading to the anomalous level-spacing statistic $P(s)$ [58].

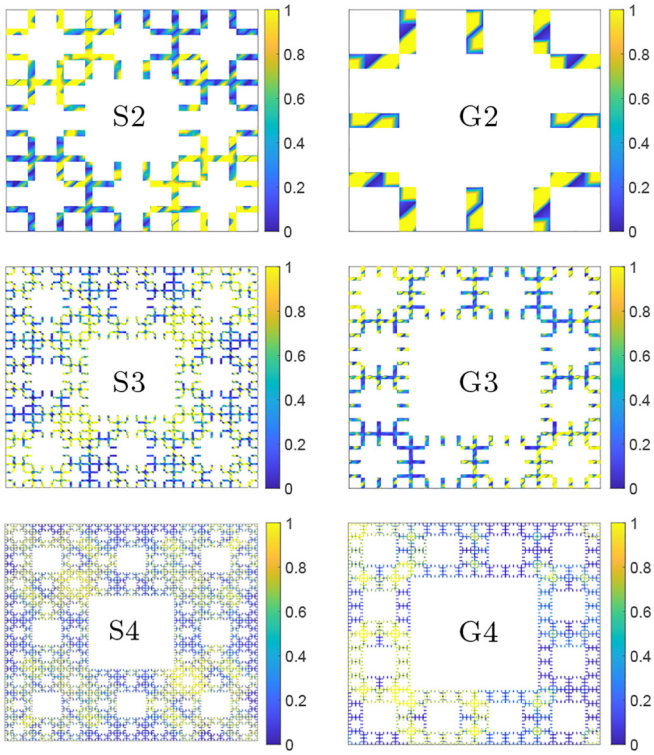

FIG. 3. The scaled state density profiles $Ar|\psi_E(i)|^2$ for the six center states closest to the band center are sequentially tagged as S2 in the SC(4, 2, 2) lattice, S3 in the SC(4, 2, 3) lattice, and S4 in the SC(4, 2, 4) lattice for the self pattern and G2 in the SC(4, 2, 2) lattice, G3 in the SC(4, 2, 3) lattice, and G4 in the SC(4, 2, 4) lattice for the gene pattern. To visualize these center states vividly, the above six lattices are scaled in the same size. The scaled factor is the lattice size Ar, and the color bar range maps from 0 to 1 (in units of Ar).

We further fix the value of g^* to compare the influence of dilation patterns on these critical states. With $g^* = 2$, the spectra of $\mathcal{D}_q^{\psi}(\psi)$ display identical contours, as seen in Figs. 2(a) and 2(d), indicating that the generator(4, 2) plays a decisive role in shaping the electronic profile within fractal lattices. This behavior becomes more pronounced when increasing g^* to 3 [Figs. 2(b) and 2(e)] or 4 [Figs. 2(c) and 2(f)]. It is noteworthy that the overall fluctuation range of $\mathcal{D}_q^{\psi}(\psi)$ in the six scenarios is predominantly influenced by the lattice size Ar of SC(4, 2, $g^* = 2$–4), where Ar is readily determined by the perimeter-area law [15,58,93].

In the six scenarios mentioned above, we further analyze six approximated center states in the energy band (specifically, $E \simeq 0$), labeled S2–S4 and G2–G4 in Fig. 3. These multifractal critical states involve wave interference on a size scale relative to the entire lattice. Five of these states (S2–S4 and G2–G3) are nearly symmetrical, which might be attributed to the disrupted translational symmetry and the discrete scaling invariance. Moreover, it is essential to highlight that, due to their unique structure, unlike in a Sierpiński gasket, the diversity between the spatial bulk state and the boundary state in these fractals is challenging, which was observed by the Hall states [61] in fractals.

The Hausdorff dimension $\mathcal{D}$ is essential for fractal objects and affects their quantum transport behaviors [59]. In our

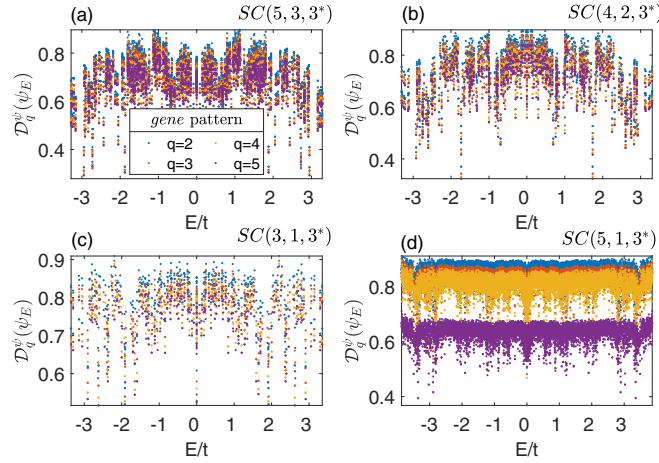

FIG. 4. $\mathcal{D}_q^{\psi}(\psi_E)$ vs critical state $\psi_E(i)$ at allowed eigenenergy E under the gene pattern. The impact of the generator(n, m) is compared by taking (a) (5,3), (b) (4,2), (c) (3,1), and (d) (5,1) with $g^* = 3$ remaining the same. Here, q is still from 2 to 5. Note that the average $\langle \mathcal{D}_2^{\psi}(\psi) \rangle$ in the four cases is 0.7312, 0.7531, 0.8035, and 0.8621, respectively.

study, $\mathcal{D}_{se}$ is influenced not only by the choice of $(r, \mathcal{N})$ but also by the generator(n, m) and geometrical hierarchy level g^*; $\mathcal{D}_{ge}$ is solely determined by its generator(n, m). If we apply the perimeter-area law [15,93] to derive $\mathcal{D}$, $\mathcal{D}_{se}$ asymptotically follows $\mathcal{D}_{se} = \log(\mathcal{N})/\log(r)$ in the self pattern (considering a large value of g^*, r, and $\mathcal{N}$; refer to Ref. [58]) and $\mathcal{D}_{ge} = \log(n^2 - m^2)/\log(n)$ in the gene pattern [58]. Note that $\mathcal{D}_{se}$ is modulated only in large fractal lattices, which makes simulation or experimental efforts difficult. We now wish to demonstrate the impact of $\mathcal{D}_{ge}$; $\mathcal{D}_{se}$ is shown in Appendix A.

$\mathcal{D}_{ge}$ is generally varied by its generator(n, m), making it easier to modulate in the case of a small g^* value. We select the sequences (5,3), (4,2), (3,1), and (5,1), resulting in $\mathcal{D}_{ge}$ gradually increasing from 1.7227 to 1.9746. In Fig. 4, we

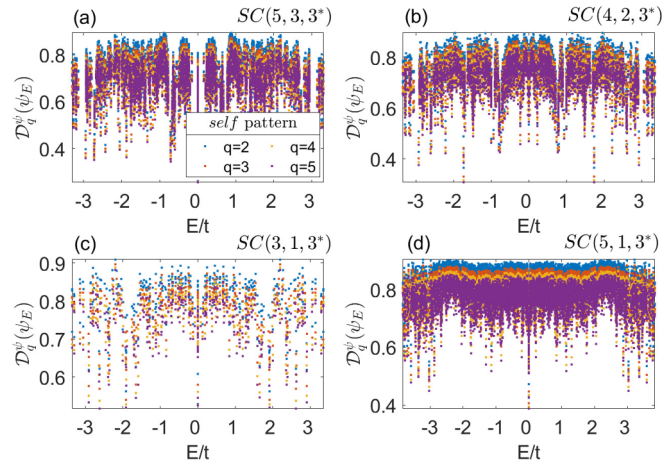

FIG. 5. Like in Fig. 4, the impact of the generator(n, m) is compared for the self pattern. Taking geometrical hierarchy level $g^* = 3$, (n, m) of (a) (5,3), (b) (4,2), (c) (3,1), and (d) (5,1) are shown. Here, q is still from 2 to 5.

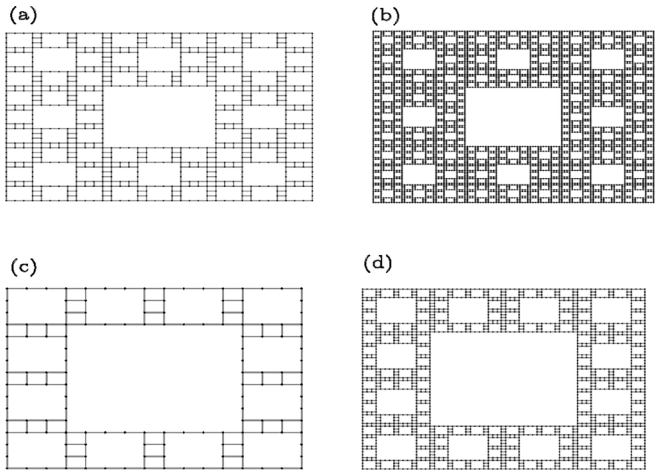

FIG. 6. Four SC$(4, 2, g^*)$ lattices in two dilation pattern. The same seed lattice of the generator$(4, 2)$ is used to construct (a) SC$(4, 2, 2)$ and (b) SC$(4, 2, 3)$ in the self pattern and (c) SC$(4, 2, 2)$ and (d) SC$(4, 2, 3)$ in the gene pattern.

set $g^* = 3$; the spectra of $\mathcal{D}_{\rm ge}$ are significantly influenced by the generator(n, m), as demonstrated in the four cases of (5, 3), (4, 2), (3, 1), and (4,2). We consider all the CSs; the average $\langle \mathcal{D}_2^{\psi}(\psi)\rangle$ for the four cases are 0.7312, 0.7531, 0.8035, and 0.8621, respectively. It is evident that the increase in $\mathcal{D}_{\rm ge}$ causes the transition from the critical state to the extended state. There is a case in the SC(5, 1, 3) lattice, as we discussed in Ref. [58], for a generator(n, m) with a large n and small m; the expanding lattices under the gene pattern can be characterized as the translation-symmetry lattices with certain pointlike or clusterlike defects. Consequently, their wave functions are slightly extended, and $\mathcal{D}_{\rm ge}$ tends towards 1.

IV. SUMMARY

In summary, by scaling the inverse participation ratio and visualizing the wave function profile, we have analyzed electronic critical states upon fractal SC(n, m, g^*) lattices that are populated under two typical patterns: the self pattern and the gene pattern. We have found that the critical states generally exhibit fragmentation behavior upon fractal SC(n, m, g^*) lattices. Therefore, it causes the electronic states to behave multicritically in fractals with $\mathcal{D}_q^{\psi}(\psi_E)$ less than 1. Note that we ascribed the above confinement effects to the hierarchal properties of the fractal structure. It could be observed by the autocorrelation function $C(t) \sim t^{-\gamma}$ and the mean-square displacement $d^2(t) \sim t^{\delta}$, with the predictions $(0 < \gamma < 1$ and $0 < \delta < 1)$ for these critical states in larger fractal lattices. For the gene pattern and the self pattern that we focused on, the fractal dimension $\mathcal{D}_2^{\psi}(\psi_E)$ is consistently greater than 0.5, which suggests that there is substantial spatial overlap among these critical states.

In addition, these states had approximate symmetry when we pinned their energy near zero. As we know, physical states can be classified according to their transport properties. The periodic Bloch functions describe conducting states in crystalline systems, and localized states in insulating systems exhibit exponential decaying. However, when discussing the critical states, things get somewhat tricky. Generally speaking, they show strong spatial fluctuations at different scales [94], occasionally accompanied by oscillatory behavior, which is evident in Sierpiński fractals. We also emphasize that in aperiodic lattices, many mechanisms possibly prevent the wave function from decaying on large scales and from being constant over the entire lattice. The following are some examples: (1) For flux-threaded Koch fractals, under the action of the commutation condition and special magnetic flux, $\psi(r_i)$ is certainly extended when pinning its eigenvalue in a special energy window [17]. (2) For the copper-mean chain [25] or period-doubling chain [26], local cluster correlation causes $\psi(r_i)$ to have a similar feature at some energy position, and some critical wave functions tend to expand in the 1D Fibonacci chain [29] and Thue-Morse lattice [48] due to short-range atom correlation. (3) Both scale invariance and the finite order of ramification cause some states to be somewhat extended in a Sierpiński gasket [27,28].

The interesting thing is that spectra of $\mathcal{D}_q^{\psi}(\psi_E)$ are determinedly modulated by the seed lattice of generator(n, m) and change slightly with the geometrical hierarchy level g^* and/or the dilation pattern. Additionally, the average fractal dimension $\mathcal{D}_2^{\psi}(\psi_E)$ will slightly increase with $\mathcal{D}_{\rm ge}$.

Note that in comparing the observed properties in irregular objects whose frontier is fractal-like, including the strong location traits in fractal drums [95,96], rich coherence of eigenwave functions is found in the Koch structure and Koch snowflake [97]. Our work provides some insight into the Sierpiński lattice. The spectra of energy level statistics [58] and $\mathcal{D}_2^{\psi}(\psi_E)$ could help with the understanding of the transport properties [59], optical spectra [98], Hall conductivity [61], even superconductivity [63] in Sierpiński lattices. At the same time, our work contributes to further study of disordered-induced localization and even many-body localization from the initial fractal-induced critical phase, and similar studies [71,99] have been carried out for quasicrystals.

ACKNOWLEDGMENTS

We thank Dr. A. Mauri for discussing this work with us. This work was supported by the National Natural Science Foundation of China (Grant No. 12174291), the Natural Science Foundation of Hubei Province, China (Grants No. 2022BAA017 and No. 2023BAA020), and the Core Facility of Wuhan University. Q.Y. acknowledges the China Scholarship Council (CSC) grant through File No. 202006270212 when attending Radboud University in the Netherlands.

APPENDIX A: THE SPECTRA OF $\mathcal{D}_q^{\psi}(\psi_E)$ IN THE SELF PATTERN

In the main text, our discussion primarily focused on the gene pattern. This pattern is crucial for understanding the behavior of a single electron in fractal lattices, particularly in terms of the fractal dimensions and the localization properties of the wave functions.

To complement this analysis, we include Fig. 5, which shows the self pattern. Figure 5 illustrates how the spectra of $\mathcal{D}_q^{\psi}(\psi_E)$ correlate with the critical states $\psi_E(i)$ across different configurations. By fixing the geometrical hierarchy level

g^*, we vary the generator(n, m), and the overall sketch profile of $\mathcal{D}_q^{\psi}(\psi_E)$ is modulated substantially [see Figs. 5(a)–5(d)]. Note that $\mathcal{D}_q^{\psi}(\psi_E)$ also reaches 0.9 in Fig. 5(d), which is due to the finite-size effect. However, $\mathcal{D}_q^{\psi}(\psi_E)$ should decrease when taking a large value of g^*; that is beyond the possible simulation ability of our computation station.

APPENDIX B: CONSTRUCTING SIERPIŃSKI CARPET SC(n, m, g^*) LATTICES

First, we need a "seed" lattice [we named it the generator(n, m), and g^* is geometric hierarchy level] and dilation pattern, including the self pattern $M_{\rm se}$ and the gene pattern $M_{\rm ge}$. Second, we construct the different types of SC(n, m, g^*) lattices using

$$\mathrm{SC}(n, m, g) = M_{\rm se,ge}(g) \otimes \mathrm{generator}(n, m), \tag{B1}$$

where g is the hierarchy level, with $M_{\rm se,ge}(g) \equiv M_{\rm se,ge}(g-1) \otimes M_{\rm se,ge}(1)$. Here, g is distinguished from g^*, which was discussed in previous work [58]. In Fig. 1, SC$(4, 2, 3^*)$ lattices are constructed with the generator$(4, 2)$ using three patterns (the third pattern is the vari pattern, which is a variation of the self pattern). Here, we focus on only the first two patterns.

For the self pattern, comprising the SC$(n, m, g^* - 1)$ lattice, the perimeter length of the SC(n, m, g^*) lattice in the g^*th iteration increases r times, and its area increases $\mathcal{N}$ times. For consistency with Ref. [58], suppose $M_{\rm se} = [1, 1, 1; 1, 0, 1; 1, 1, 1]$ with $r = 3$ and $\mathcal{N} = 8$ [see Figs. 6(a) and 6(b)]. For the gene pattern, the pattern depends on the seed lattice of the generator$(4, 2)$, and we have $M_{\rm ge} = [1, 1, 1, 1; 1, 0, 0, 1; 1, 0, 0, 1; 1, 1, 1, 1]$ [see Figs. 6(c) and 6(d)].

[1] C. Kittel, *Introduction to Solid State Physics*, 8th ed. (Wiley, Hoboken, NJ, 2021).
[2] N. W. Ashcroft and N. D. Mermin, *Solid State Physics* (Holt, Rinehart and Winston, New York, 1976).
[3] S. V. Vonsovsky and M. I. Katsnelson, *Quantum Solid State Physics* (Springer-Verlag, Berlin, Heidelberg, 1989).
[4] P. Phillips, *Advanced Solid State Physics* (Cambridge University Press, Cambridge, 2012).
[5] M. El-Batanouny, *Advanced Quantum Condensed Matter Physics: One-Body, Many-Body, and Topological Perspectives* (Cambridge University Press, Cambridge, 2020).
[6] N. F. Mott and E. A. Davis, *Electronic Processes in Non-crystalline Materials* (Oxford University Press, Oxford, 1971).
[7] J. M. Ziman, *Models of Disorder* (Cambridge University Press, Cambridge, 1979).
[8] I. M. Lifshitz, S. A. Gredeskul, and L. A. Pastur, *Introduction to the Theory of Disordered Systems* (Wiley, New York, 1988).
[9] D. Shechtman, I. Blech, D. Gratias, and J. W. Cahn, Metallic phase with long-range orientational order and no translational symmetry, Phys. Rev. Lett. **53**, 1951 (1984).
[10] H. Tsunetsugu, T. Fujiwara, K. Ueda, and T. Tokihiro, Electronic properties of the Penrose lattice. I. Energy spectrum and wave functions, Phys. Rev. B **43**, 8879 (1991).
[11] H. Tsunetsugu and K. Ueda, Electronic properties of the Penrose lattice. II. Conductance at zero temperature, Phys. Rev. B **43**, 8892 (1991).
[12] F. P. M. Beenker, Algebraic theory of non-periodic tilings of the plane by two simple building blocks: A square and a rhombus, Ph.D. thesis, Eindhoven University of Technology, 1982.
[13] B. Grünbaum and G. C. Shephard, *Tilings and Patterns* (Courier Dover, 1987).
[14] B. B. Mandelbrot, *The Fractal Geometry of Nature* (Freeman New York, 1982), Vol. 1.
[15] J. Feder, *Fractals* (Springer Science & Business Media, New York, 2013).
[16] T. Nakayama and K. Yakubo, *Fractal Concepts in Condensed Matter Physics* (Springer Science & Business Media, New York, 2003), Vol. 140.
[17] S. Biswas and A. Chakrabarti, Complete escape from localization on a hierarchical lattice: A Koch fractal with all states extended, Phys. Rev. B **108**, 125430 (2023).
[18] P. W. Anderson, Absence of diffusion in certain random lattices, Phys. Rev. **109**, 1492 (1958).
[19] F. Evers and A. D. Mirlin, Anderson transitions, Rev. Mod. Phys. **80**, 1355 (2008).
[20] E. Domany, S. Alexander, D. Bensimon, and L. P. Kadanoff, Solutions to the Schrödinger equation on some fractal lattices, Phys. Rev. B **28**, 3110 (1983).
[21] Q. Niu and F. Nori, Renormalization-group study of one-dimensional quasiperiodic systems, Phys. Rev. Lett. **57**, 2057 (1986).
[22] A. Chakrabarti and S. N. Karmakar, Renormalization-group method for exact Green's functions of self-similar lattices: Application to generalized Fibonacci chains, Phys. Rev. B **44**, 896 (1991).
[23] X. H. Yan, J. X. Zhong, J. R. Yan, and J. Q. You, Renormalization group of generalized Fibonacci lattices, Phys. Rev. B **46**, 6071 (1992).
[24] J. Q. You, J. R. Yan, J. X. Zhong, and X. H. Yan, Local electronic properties of two-dimensional Penrose tilings: A renormalization-group approach, Phys. Rev. B **45**, 7690 (1992).
[25] S. Sil, S. N. Karmakar, R. K. Moitra, and A. Chakrabarti, Extended states in one-dimensional lattices: Application to the quasiperiodic copper-mean chain, Phys. Rev. B **48**, 4192 (1993).
[26] A. Chakrabarti, S. N. Karmakar, and R. K. Moitra, Renormalization-group analysis of extended electronic states in one-dimensional quasiperiodic lattices, Phys. Rev. B **50**, 13276 (1994).
[27] A. Chakrabarti, Exact results for infinite and finite Sierpinski gasket fractals: Extended electron states and transmission properties, J. Phys.: Condens. Matter **8**, 10951 (1996).
[28] S. Biswas and A. Chakrabarti, Designer quantum states on a fractal substrate: Compact localization, flat bands and the edge modes, Phys. E (Amsterdam, Neth.) **153**, 115762 (2023).
[29] E. Maciá and F. Domínguez-Adame, Physical nature of critical wave functions in Fibonacci systems, Phys. Rev. Lett. **76**, 2957 (1996).
[30] A. Eilmes, R. Römer, and M. Schreiber, The two-dimensional Anderson model of localization with random hopping, Eur. Phys. J. B **1**, 29 (1998).

[31] *Physical Properties of Quasicrystals*, edited by Z. M. Stadnik (Springer Science & Business Media, New York, 2012).

[32] A. Jagannathan, The Fibonacci quasicrystal: Case study of hidden dimensions and multifractality, Rev. Mod. Phys. **93**, 045001 (2021).

[33] F. J. Dyson, Statistical theory of the energy levels of complex systems. I, J. Math. Phys. **3**, 140 (1962).

[34] M. L. Mehta, *Random Matrices* (Academic, New York 1991).

[35] K. Efetov, *Supersymmetry in Disorder and Chaos* (Cambridge University Press, Cambridge, 1999).

[36] R. Cafiero, A. Gabrielli, M. Marsili, M. A. Muñoz, and L. Pietronero, Generalized dielectric breakdown model, Phys. Rev. B **60**, 786 (1999).

[37] T. Nakayama, K. Yakubo, and R. L. Orbach, Dynamical properties of fractal networks: Scaling, numerical simulations, and physical realizations, Rev. Mod. Phys. **66**, 381 (1994).

[38] A. Mirlin, Statistics of energy levels and eigenfunctions in disordered systems, Phys. Rep. **326**, 259 (2000).

[39] I. K. Zharekeshev and B. Kramer, Scaling of level statistics at the disorder-induced metal-insulator transition, Phys. Rev. B **51**, 17239 (1995).

[40] K. R. Amin, R. Nagarajan, R. Pandit, and A. Bid, Multifractal conductance fluctuations in high-mobility graphene in the integer quantum Hall regime, Phys. Rev. Lett. **129**, 186802 (2022).

[41] A. L. R. Barbosa, T. H. V. de Lima, I. R. R. González, N. L. Pessoa, A. M. S. Macêdo, and G. L. Vasconcelos, Turbulence hierarchy and multifractality in the integer quantum Hall transition, Phys. Rev. Lett. **128**, 236803 (2022).

[42] X. Yang, W. Zhou, Q. Yao, P. Lv, Y. Wang, and S. Yuan, Electronic properties and quantum transport in functionalized graphene Sierpinski-carpet fractals, Phys. Rev. B **105**, 205433 (2022).

[43] M. Kohmoto and B. Sutherland, Electronic states on a Penrose lattice, Phys. Rev. Lett. **56**, 2740 (1986).

[44] N. Macé, A. Jagannathan, P. Kalugin, R. Mosseri, and F. Piéchon, Critical eigenstates and their properties in one- and two-dimensional quasicrystals, Phys. Rev. B **96**, 045138 (2017).

[45] W. Zhou and S. Yuan, A time-dependent random state approach for large-scale density functional calculations, Chin. Phys. Lett. **40**, 027101 (2023).

[46] M. Quilichini, Phonon excitations in quasicrystals, Rev. Mod. Phys. **69**, 277 (1997).

[47] M. Kohmoto, B. Sutherland, and C. Tang, Critical wave functions and a Cantor-set spectrum of a one-dimensional quasicrystal model, Phys. Rev. B **35**, 1020 (1987).

[48] A. Chakrabarti, S. N. Karmakar, and R. K. Moitra, Role of a new type of correlated disorder in extended electronic states in the Thue-Morse lattice, Phys. Rev. Lett. **74**, 1403 (1995).

[49] B. Sutherland, Self-similar ground-state wave function for electrons on a two-dimensional Penrose lattice, Phys. Rev. B **34**, 3904 (1986).

[50] G. R. Newkome, P. Wang, C. N. Moorefield, T. J. Cho, P. P. Mohapatra, S. Li, S.-H. Hwang, O. Lukoyanova, L. Echegoyen, J. A. Palagallo, V. Iancu, and S.-W. Hla, Nanoassembly of a fractal polymer: A molecular "Sierpinski hexagonal gasket," Science **312**, 1782 (2006).

[51] J. A. Fan, W.-H. Yeo, Y. Su, Y. Hattori, W. Lee, S.-Y. Jung, Y. Zhang, Z. Liu, H. Cheng, L. Falgout, M. Bajema, T. Coleman, D. Gregoire, R. J. Larsen, Y. Huang, and J. A. Rogers, Fractal design concepts for stretchable electronics, Nat. Commun. **5**, 3266 (2014).

[52] J. Shang, Y. Wang, M. Chen, J. Dai, X. Zhou, J. Kuttner, G. Hilt, X. Shao, J. M. Gottfried, and K. Wu, Assembling molecular Sierpiński triangle fractals, Nat. Chem. **7**, 389 (2015).

[53] C. Liu, Y. Zhou, G. Wang, Y. Yin, C. Li, H. Huang, D. Guan, Y. Li, S. Wang, H. Zheng, C. Liu, Y. Han, J. W. Evans, F. Liu, and J. Jia, Sierpiński structure and electronic topology in Bi thin films on InSb(111)B surfaces, Phys. Rev. Lett. **126**, 176102 (2021).

[54] Z. Yang, E. Lustig, Y. Lumer, and M. Segev, Photonic Floquet topological insulators in a fractal lattice, Light: Sci. Appl. **9**, 128 (2020).

[55] L. Song, H. Yang, Y. Cao, and P. Yan, Realization of the square-root higher-order topological insulator in electric circuits, Nano Lett. **20**, 7566 (2020).

[56] J. Li, Y. Sun, Q. Mo, Z. Ruan, and Z. Yang, Fractality-induced topological phase squeezing and devil's staircase, Phys. Rev. Res. **5**, 023189 (2023).

[57] S. N. Kempkes, M. R. Slot, S. E. Freeney, S. J. M. Zevenhuizen, D. Vanmaekelbergh, I. Swart, and C. M. Smith, Design and characterization of electrons in a fractal geometry, Nat. Phys. **15**, 127 (2019).

[58] Q. Yao, X. Yang, A. A. Iliasov, M. I. Katsnelson, and S. Yuan, Energy-level statistics in planar fractal tight-binding models, Phys. Rev. B **107**, 115424 (2023).

[59] E. van Veen, S. Yuan, M. I. Katsnelson, M. Polini, and A. Tomadin, Quantum transport in Sierpinski carpets, Phys. Rev. B **93**, 115428 (2016).

[60] T. Westerhout, E. van Veen, M. I. Katsnelson, and S. Yuan, Plasmon confinement in fractal quantum systems, Phys. Rev. B **97**, 205434 (2018).

[61] A. A. Iliasov, M. I. Katsnelson, and S. Yuan, Hall conductivity of a Sierpiński carpet, Phys. Rev. B **101**, 045413 (2020).

[62] The fractal-induced critical phase could be driven to the localization phase by increasing the disorder strength, and one would observe the energy-level-correlation spectra gradually transitioning from the Wigner-like distribution to the Poisson distribution and multifractal critical states trend to localized states.

[63] A. A. Iliasov, M. I. Katsnelson, and A. A. Bagrov, Strong enhancement of superconductivity on finitely ramified fractal lattices, arXiv:2310.11497.

[64] P. G. Harper, Single band motion of conduction electrons in a uniform magnetic field, Proc. Phys. Soc. Sect. A **68**, 874 (1955).

[65] S. Aubry and G. André, Analyticity breaking and Anderson localization in incommensurate lattices, Ann. Isr. Phys. Soc. **3**, 18 (1980).

[66] P. G. Harper, The general motion of conduction electrons in a uniform magnetic field, with application to the diamagnetism of metals, Proc. Phys. Soc. Sect. A **68**, 879 (1955).

[67] C. M. Soukoulis and E. N. Economou, Fractal character of eigenstates in disordered systems, Phys. Rev. Lett. **52**, 565 (1984).

[68] P. de Vries, H. De Raedt, and A. Lagendijk, Localization of waves in fractals: Spatial behavior, Phys. Rev. Lett. **62**, 2515 (1989).

[69] I. Varga, E. Hofstetter, and J. Pipek, One-parameter superscaling at the metal-insulator transition in three dimensions, Phys. Rev. Lett. **82**, 4683 (1999).

[70] J. Pipek and I. Varga, Universal classification scheme for the spatial-localization properties of one-particle states in finite, d-dimensional systems, Phys. Rev. A **46**, 3148 (1992).

[71] Y. Wang, X. Xia, L. Zhang, H. Yao, S. Chen, J. You, Q. Zhou, and X.-J. Liu, One-dimensional quasiperiodic mosaic lattice with exact mobility edges, Phys. Rev. Lett. **125**, 196604 (2020).

[72] M. Janssen, Statistics and scaling in disordered mesoscopic electron systems, Phys. Rep. **295**, 1 (1998).

[73] M. Janssen, Multifractal analysis of broadly-distributed observables at criticality, Int. J. Mod. Phys. B **8**, 943 (1994).

[74] The stairlike density of states, $\rho(E) = 1/Ar \sum_{k=1}^{Ar} \delta(E - E_k)$, will be blurred with a smooth function $g_\sigma(t)$. When we regularize the Dirac function $\delta(t)$ by a Gaussian or Lorentz function $g_\sigma(t)$, $\rho_\sigma(E)$ usually has a smoother curve.

[75] I. Guarneri, On an estimate concerning quantum diffusion in the presence of a fractal spectrum, Europhys. Lett. **21**, 729 (1993).

[76] G. De Tomasi, S. Bera, A. Scardicchio, and I. M. Khaymovich, Subdiffusion in the Anderson model on the random regular graph, Phys. Rev. B **101**, 100201(R) (2020).

[77] B. O'Shaughnessy and I. Procaccia, Diffusion on fractals, Phys. Rev. A **32**, 3073 (1985).

[78] L. Guidoni, B. Dépret, A. di Stefano, and P. Verkerk, Atomic diffusion in an optical quasicrystal with five-fold symmetry, Phys. Rev. A **60**, R4233 (1999).

[79] L. Basnarkov and V. Urumov, Diffusion on Archimedean lattices, Phys. Rev. E **73**, 046116 (2006).

[80] M. A. Di Muro and M. Hoyuelos, Diffusion on a lattice: Transition rates, interactions, and memory effects, Phys. Rev. E **106**, 014139 (2022).

[81] *Physical Properties of Quasicrystals*, edited by Z. M. Stadnik (Springer Science & Business Media, New York, 2012), Vol. 126.

[82] T. Fujiwara, M. Kohmoto, and T. Tokihiro, Multifractal wave functions on a Fibonacci lattice, Phys. Rev. B **40**, 7413 (1989).

[83] T. Tokihiro, T. Fujiwara, and M. Arai, Exact eigenstates on a two-dimensional Penrose lattice and their fractal dimensions, Phys. Rev. B **38**, 5981 (1988).

[84] T. Fujiwara, Electronic structure in the Al-Mn alloy crystalline analog of quasicrystals, Phys. Rev. B **40**, 942 (1989).

[85] T. Rieth and M. Schreiber, Numerical investigation of electronic wave functions in quasiperiodic lattices, J. Phys.: Condens. Matter **10**, 783 (1998).

[86] Y. Gefen, Y. Meir, B. B. Mandelbrot, and A. Aharony, Geometric implementation of hypercubic lattices with noninteger dimensionality by use of low lacunarity fractal lattices, Phys. Rev. Lett. **50**, 145 (1983).

[87] B. Lin, Classification and universal properties of Sierpinski carpets, J. Phys. A **20**, L163 (1987).

[88] Y. Hatsugai and M. Kohmoto, Energy spectrum and the quantum Hall effect on the square lattice with next-nearest-neighbor hopping, Phys. Rev. B **42**, 8282 (1990).

[89] X. Cai, L.-J. Lang, S. Chen, and Y. Wang, Topological superconductor to Anderson localization transition in one-dimensional incommensurate lattices, Phys. Rev. Lett. **110**, 176403 (2013).

[90] F. Liu, S. Ghosh, and Y. D. Chong, Localization and adiabatic pumping in a generalized Aubry-André-Harper model, Phys. Rev. B **91**, 014108 (2015).

[91] Y. Wang, L. Zhang, S. Niu, D. Yu, and X.-J. Liu, Realization and detection of nonergodic critical phases in an optical Raman lattice, Phys. Rev. Lett. **125**, 073204 (2020).

[92] T. Xiao, D. Xie, Z. Dong, T. Chen, W. Yi, and B. Yan, Observation of topological phase with critical localization in a quasi-periodic lattice, Sci. Bull. **66**, 2175 (2021).

[93] B. Mandelbrot, *Fractals* (Freeman, San Francisco, 1977).

[94] *Applications of Random Matrices in Physics*, edited by É. Brézin, V. Kazakov, D. Serban, P. Wiegmann, and A. Zabrodin (Springer Science & Business Media, New York, 2006), Vol. 221.

[95] C. Even, S. Russ, V. Repain, P. Pieranski, and B. Sapoval, Localizations in fractal drums: An experimental study, Phys. Rev. Lett. **83**, 726 (1999).

[96] S. Homolya, C. F. Osborne, and I. D. Svalbe, Density of states for vibrations of fractal drums, Phys. Rev. E **67**, 026211 (2003).

[97] A. Adrover and F. Garofalo, Scaling of the density of state of the weighted Laplacian in the presence of fractal boundaries, Phys. Rev. E **81**, 027202 (2010).

[98] E. van Veen, A. Tomadin, M. Polini, M. I. Katsnelson, and S. Yuan, Optical conductivity of a quantum electron gas in a Sierpinski carpet, Phys. Rev. B **96**, 235438 (2017).

[99] X.-C. Zhou, Y. Wang, T.-F. J. Poon, Q. Zhou, and X.-J. Liu, Exact new mobility edges between critical and localized states, Phys. Rev. Lett. **131**, 176401 (2023).